

Manufacturing 1×16 MMI vertical coupling optical splitter based on composite fabricating method

QING TAO^{1,2}, LIANGPENG WEI¹, SIHAO XIE^{1,2,*}

¹*School of Mechanical Engineering, Hubei University of Technology, Wuhan 430068, China*

²*Hubei Key Laboratory of Modern Manufacturing Quantity Engineering, School of Mechanical Engineering, Hubei University of Technology, Wuhan, Hubei, 430068, P.R. China*

In this paper, a composite fabricating method was proposed for manufacturing 1×16 MMI vertical coupling optical splitter with Su8 core layer and air cladding layer. The femtosecond laser composite fabrication combined simultaneous spatial and temporal focusing technology with traditional lens focusing method. Compared with the traditional lens focusing method, this composite fabricating method improved the processing accuracy. The diameter of incident aperture was 5 mm, the distance of grating pairs was 500 mm, and the angle of grating pairs was 48°, the groove density of gratings was 1500 lines/mm. The femtosecond laser wavelength was 800 nm, wavelength width was 8 nm, and, 100 fs pulses with a maximum pulse energy of 0.4 mJ at a repetition rate of 10 kHz. The testing results showed average insertion loss of each output port was 18.34 dB, and non-uniformity was 0.1988 dB in the optical splitter. This met requirements of vertical coupling optical interconnection for the EOPCB.

(Received May 31, 2022; accepted October 5, 2022)

Keywords: Vertical coupling, Composite fabricating method, Simultaneous spatial and temporal focusing

1. Introduction

With the development of optoelectronic integrated circuits, the demand for optical interconnection communication between chips based on the circuit board level was growing. FR4 material were circuit layers in the traditional electro-optical printed circuit board (EOPCB). An optical waveguide layer composed of polymer material was integrated between FR4 layers, which was used for unidirectional point-to-point information transmission between VCSEL laser and PIN detector [1-3]. As the size of electronic chip was getting smaller and smaller, more chips could be integrated on the circuit board, and the demand for single-point-to-multipoint information transmission was also increasing. Therefore, this paper proposed a solution to this problem by integrating a 1×16 MMI optical splitter in the optical waveguide layer. The coupling of VCSEL laser and PIN detector of traditional optoelectronic circuit board to the optical waveguide layer was realized through special optical fibers or special optical structures. Because the optical waveguide was sandwiched between the FR4 layers, the expansion coefficients of two materials were different, which was easy to crack and fall off during working for a long time. A 1×16 MMI air-cladding optical splitter layer based on silica substrate was designed, which was fixed by bolts. And, the input and output ends of 1×16 MMI optical

splitter layer were made into a 45° coupled waveguide structure, and the transmission loss between chips was low, which did not affect the optical communication. Currently, the methods, which fabricating polymer optical waveguides for EOPCBs, included ultraviolet photolithography [4-5], ion etching [6-7], mosquito method [8-9], femtosecond laser etching [10-11], etc. However, ultraviolet photolithography, ion etching and mosquito method were relatively expensive and these processing were more complicated [12-15].

Moreover, the diversity of device structures and physical, chemical, or optical properties, some techniques were only applicable to specific materials. Among these solutions, femtosecond laser writing had been recognized as an efficient tool to fabricate optical devices in the Su8 polymer owing to the powerful 3D engineering capability and microscale fabrication [16-17]. Quite extensive studies had been performed on this topic, and the materials had also been extended to ceramics, organic materials, and so on [18–22]. However, the precision of traditional femtosecond laser etching was low [23-25]. The femtosecond laser composite fabricating method was proposed to improve the processing accuracy and it was more suitable for the fabrication of optical waveguide devices [26-28]. In this work, we concentrated on the new femtosecond laser composite fabricating technique. For specific geometries of optical splitter, the manufacturing process was

precisely adjusted. The communication performance of EOPCB was significantly improved.

2. Design of improved EOPCB

2.1. The principle of multimode interference optical splitter

The principle of multimode interference optical splitter was the self-imaging effect [29-31]. When light entered a multi-mode waveguide, various guided modes in the waveguide would be excited. Because the propagation constants of different guided modes were different, when the light propagated, phase difference and mutual interference would occur. Then, output mirror images of light field would appear in a specific position where the propagation constants of different orders of guided modes satisfied a self-imaging effect. N output lights could be obtained by setting N output waveguides at the specific positions, then, the optical splitter could be completed.

At the input region of multimode interference, the input field could be written as a linear combination of all eigenmodes:

$$f(x, z=0) = \sum_m c_m \phi_m(x) \quad (1)$$

$\phi_m(x)$ was the m-th order eigenmode of MMI part, and c_m was the weight coefficient. Then, the light field at z was,

$$f(x, z) = \sum_m c_m \phi_m(x) e^{-i\beta_m z} \quad (2)$$

where β_m was the propagation constant of the m-th order eigenmode.

Two assumptions were put forward in the self-imaging effect: one was to assume that the k_{ey} was much smaller than $k_0 n_r (k_{ey}^2 + \beta_m^2 = k_0^2 n_r^2)$, where k_0 was the wave vector in the vacuum, and the k_{ey} was the y component of wave vector. Another was to assume that the effective width of m-th order eigenmode was equal to the effective width of 0-th order eigenmode, that is, $W_e^m = W_e^0$. The formula (2) could be rewritten as,

$$f(x, z) = \exp(i\beta_0 z) \sum_m c_m \phi_m(x) \exp\left[i \frac{m(m+2)\pi}{3L_\pi} z\right] \quad (3)$$

where, L_π was the beat length,

$$L_\pi = \frac{\pi}{\beta_0 - \beta_1} \quad (4)$$

The positions of N image could be obtained by formula (3), when N images were obtained, the total length L was,

$$L = \frac{3L_\pi}{N} \quad (5)$$

The coordinate positions (x_i) of output waveguides were as follows,

$$x_i = \frac{[2i - (N+1)]W_e^0}{2N} \quad (6)$$

After the width of MMI multi-mode interference region was determined, the length of MMI multi-mode interference region and the coordinate positions of output waveguide could be calculated by the formulas (5) and (6). According to formula (4), the beat length was obtained.

$$L_\pi = \frac{\pi}{\beta_0 - \beta_1} = \frac{4n_r W_e^2}{3\lambda_0} \quad (7)$$

where, n_r and W_e represented the effective refractive index and effective width of MMI, respectively. Then, the mode distribution at the output end of multimode waveguide could be obtained by the guided mode transmission method.

$$\varphi(x, L) = \sum_{m=0}^{m-1} c_m \phi_m(x) \exp\left[j \frac{m(m+2)\pi}{3L_\pi} L\right] \quad (8)$$

For a 1×N optical splitter, the input waveguide was set at the middle of multimode waveguide (x=0), the purpose was to restrict the multimode waveguide to excite only even modes (m=0, 2, 4, 6, 8...), the interference was symmetrical. So, when the formula was established,

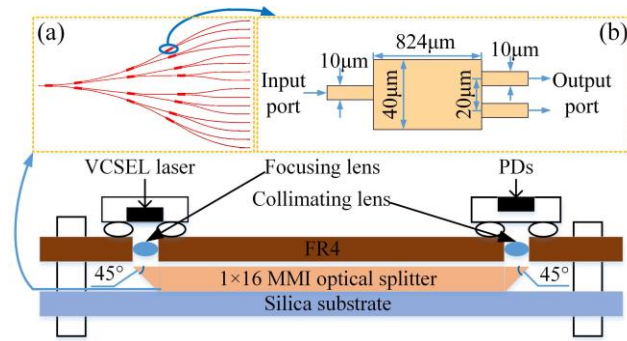
$$L = \frac{3L_\pi}{4N} \quad (9)$$

N image could appear at the end of multimode waveguide. Then, a 1×N optical splitter was also designed.

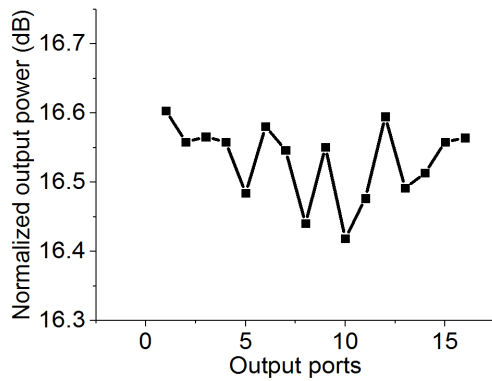
2.2. Design of 1×16 MMI optical splitter

A 1×16 MMI air-cladding Su8 polymeric optical splitter was designed for EOPCB [32] in Fig. 1. Electronic components were mounted on the FR4 layer. Silica was the substrate layer. 1×16 MMI optical splitter was sandwiched between two layers. The width of MMI waveguide was 40 μm, its length was 824 μm, the distance between two output waveguides was 20 μm. The cladding of optical splitter was air, its refractive index

was 1 @ 1550 nm. The refractive index of silica glass was 1.45 @ 1550 nm. The core layer was Su8 polymer, its refractive index was 1.566 @1550 nm. The length of 1×16 optical splitter was 2.2 cm, the spacing of output waveguide was 127 μm .



(a) Structure of EOPCB



(b) Normalized output power for each port

Fig. 1. Design of 1×16 MMI optical splitter (color online)

The structure of 1×16 MMI vertical coupled optical splitter was shown in Fig. 1(a). The cross section of optical splitter was 10 μm ×10 μm . The input and output ports of optical splitter were cut to 45°. Normalized output powers were simulated in Fig. 1(b), the average normalized output power was 16.53 dB, and the non-uniformity was 0.0486.

2.3. Design of 45° coupled waveguide structure

The 1550 nm laser emitted by VCSEL was converged by focusing lens and vertically coupled into 45° coupled waveguide structure in Fig. 2. Then, laser transmitted along the 1×16 optical splitter. Output lasers were vertically reflected to collimating lens, and the beams were received by multiple photodetectors to realize optical communication at the circuit board [33].

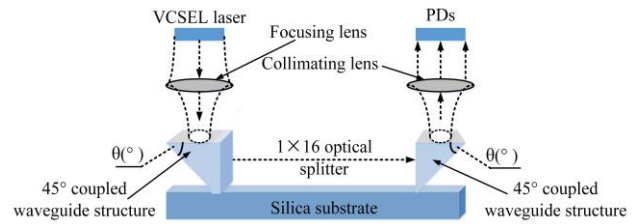


Fig. 2. 45° coupled waveguide structure

When the angle (θ) changed, it would affect the optical power coupling efficiency between VCSEL laser and PDs. Assuming that there was no loss between VCSEL laser and PDs, the normalized coupling efficiency (δ) was defined as 1 [34–35].

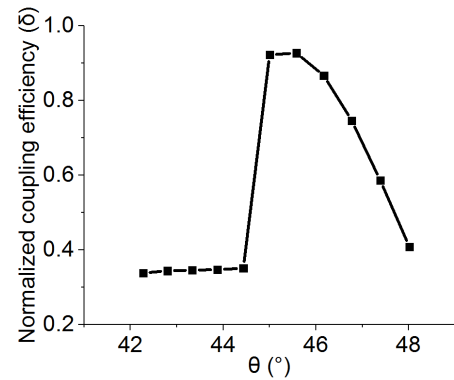


Fig. 3. The relationship between angle (θ) and normalized coupling efficiency (δ)

When angle (θ) changed from 42° to 44.5°, normalized coupling efficiency (δ) varied from 0.338 to 0.351, and deviation of δ was not obvious in Fig. 3. When angle (θ) changed from 44.5° to 45°, δ increased rapidly from 0.351 to 0.97. When angle (θ) changed from 45° to 45.9°, δ was still greater than 0.9. When angle (θ) gradually increased from 45.9° to 48°, δ decreased sharply. Only when $\theta \in [44.8^\circ, 45.9^\circ]$, δ was greater than 90%.

3. Femtosecond laser composite fabrication

3.1. The principle of simultaneous spatial and temporal focusing

Here, it was assumed that the incident femtosecond laser pulse had a circular Gaussian profile, namely, their beam waists along the major axis (w_x) and the minor axis (w_y) were the same. The ellipticity of Gaussian beam could be tuned with a narrow aperture, as illustrated in Fig. 4. Here, d_g was the distance between gratings pairs. Angle i was the input angle of Gaussian light, and angle r was the output angle of Gaussian light [36–40].

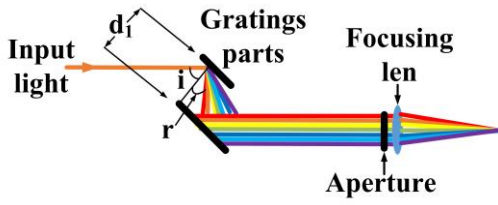


Fig. 4. Simultaneous spatial and temporal focusing (color online)

Firstly, the normalized light field of spatially dispersed pulse A_1 at the entrance aperture of objective lens could be expressed as,

$$A_1(x, y, \omega) = \frac{A_0}{\sqrt{\pi}\Omega} \exp\left(-\frac{(\omega - \omega_0)^2}{\Omega^2}\right) \times \exp\left(-\frac{x - \Delta x(\omega)^2}{2W_x^2}\right) \exp\left(-\frac{y^2}{2W_y^2}\right) \quad (10)$$

where, A_0 was optical field amplitude, ω_0 was carrier frequency, $\sqrt{2}\Omega$ was bandwidth of femtosecond pulse measured at $1/e^2$, $\sqrt{2}W_x$ and $\sqrt{2}W_y$ were beam waists along major and minor axes measured at $1/e^2$, respectively. Neglecting the high-order chirp induced by the grating pair, the linear shift of each spectral component at the entrance aperture could be written as $\Delta x(\omega) \approx \alpha(\omega - \omega_0)$.

After passing through the objective lens, the light field could be written as,

$$A_2(x, y, \omega) = A_1(x, y, \omega) \exp\left(-ik \frac{x^2 + y^2}{2f}\right) \quad (11)$$

where, k was the wave vector and f was the focal length of objective lens. Then, propagating distance z from the lens, light field could be described by the Fresnel diffraction equation,

$$A_3(x, y, z, \omega) = \frac{\exp(ikz)}{i\lambda z} \times \int \int_{-\infty}^{\infty} A_2(\xi, \eta, \omega) \times \exp\left[ik \frac{(x - \xi)^2 + (y - \eta)^2}{2z}\right] d\xi d\eta \quad (12)$$

Performing inversed Fourier transformation of A_3 , light field in the time domain could be written as,

$$A_4(x, y, z, t) = \int_{-\infty}^{\infty} A_3(x, y, z, \omega) \exp(-i\omega t) d\omega \quad (13)$$

Then, three dimensions peak intensity could be calculated by substituting $z = f$ and $t \approx 0$ into equation (13),

$$I(x, y, z, t) = |A_4|^2 \quad (14)$$

The grating pair was ruled with σ . The first-order diffraction must satisfy the following equation,

$$\sin \gamma = \sin i - \lambda / \sigma \quad (15)$$

where, λ_0 and ω_0 were the central wavelength and the central frequency, respectively. And, $\Delta\lambda$ was wavelength width. Hence, the coefficient was

$$\alpha = -d_1 \lambda_0 \cos i / (\sigma \omega_0 \cos^3 \gamma) \quad (16)$$

From above formula, the optical field power distribution near the focus were calculated in Fig. 5. At the focal point, it could be seen that the diameter of optical spot was $0.2 \mu\text{m}$ in Fig. 5(a). The optical field power distribution was approximately a long racetrack type, its long side was $2 \mu\text{m}$ and its short side was $0.2 \mu\text{m}$ in Fig. 5(b)-5(c).

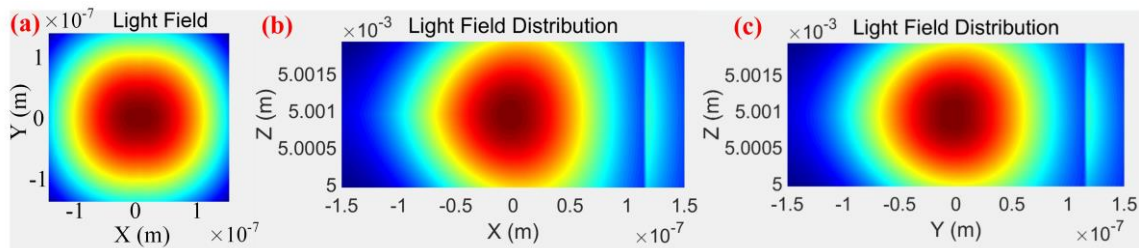


Fig. 5. Optical field power distribution near the focus (color online)

3.2. Composite fabricating method

Firstly, the silica substrate was boiled in 5% dilute sulfuric acid for 4 hours in a fume hood to remove impurities and roughness on the surface and made it smooth. Then, the silica substrate was placed in ultrasonic cleaning for 5-10 minutes and it was dried

with nitrogen. The silica substrate was evenly spun Su8 adhesive on its surface and thickness of Su8 adhesive was $10 \mu\text{m}$. Afterwards, the composite fabricating system was used in Fig. 6, which had two sets of independent light paths, and they needed to switch according to the computer's program for composite processing. Light path 1 consisted of several parts, which were attenuator,

rotatable reflector, shutter, reflector, collimating lens, grating pair, aperture, focusing lens. When rotatable reflector blocked the output light of attenuator, light path 1 was in the working state. At this time, light path 1 was finely used for the outline of optical splitter and edges. Light path 2 consisted of several parts, which were attenuator, rotatable reflector, reflector, collimating lens, aperture, focusing lens. When rotatable reflector didn't block the output light of attenuator, light path 2 was in the working state. Light path 2 was used for the inner processing of outline of optical splitter and the processing near the edges.

Because light path 1 could break through the diffraction limit, the diameter of focal spot could theoretically be smaller than $0.3\ \mu\text{m}$, light path 1 was firstly used to ablate the contour of optical splitter and these edges of contour. Light path 2 was used to ablate the inside part of optical splitter outline and near the edges of contour, which formed a 1×16 MMI optical splitter without 45° coupled waveguide structure. For manufacturing 45° coupled waveguide structure, the side face of optical splitter ports was in the focal plane. Light path 1 was used to ablate lines of different depths along the 45° angle on the end face. 1×16 MMI vertical coupled optical splitter was fabricated with above steps.

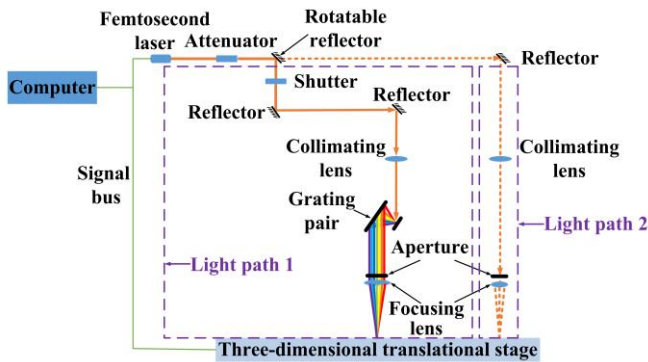
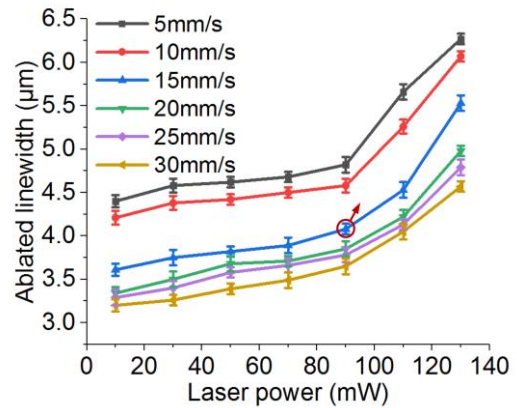


Fig. 6. The femtosecond laser composite fabricating system (color online)

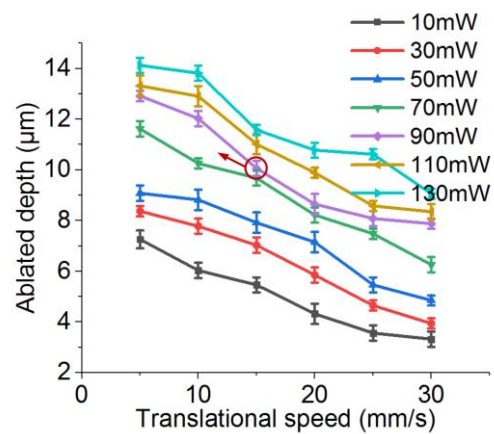
The resolution of three-dimensional translational stage was $0.1\ \mu\text{m}$, which drove the samples to change position. The focusing lens was a 40X objective lens with numerical aperture $\text{NA}=0.6$. The femtosecond laser (Coherent Libra HE) was with a center wavelength of $800\ \text{nm}$, 100fs pulses with a maximum pulse energy of $0.4\ \text{mJ}$ at a repetition rate of $10\ \text{kHz}$, and beam quality factor $M^2 < 1.3$. Femtosecond laser pulse had a Gaussian profile, the major and minor axis waist were $5\ \text{mm}$. The distance (d_1) of gratings pair was $500\ \text{mm}$. The input angle (i) of Gaussian light was 48° . Focal length was $5\ \text{mm}$. The grating pair was ruled with $1500\ \text{lines/mm}$. The wavelength width was $8\ \text{nm}$. The optical spot diameter was about $0.3\ \mu\text{m}$.

4. Results and discussion

Laser power and translational speed had greater impacts on the line-depth and linewidth [41-43]. The linewidth was closer to $4\ \mu\text{m}$ and the line depth was closer to $10\ \mu\text{m}$ after scan once. The optimal laser power and translational speed were obtained by cross-experiments. Laser power was set within $30\ \text{mW}$ to $130\ \text{mW}$, and the translational speed was set between $5\ \text{mm/s}$ and $30\ \text{mm/s}$, results of cross-experiments were obtained in Fig. 7.



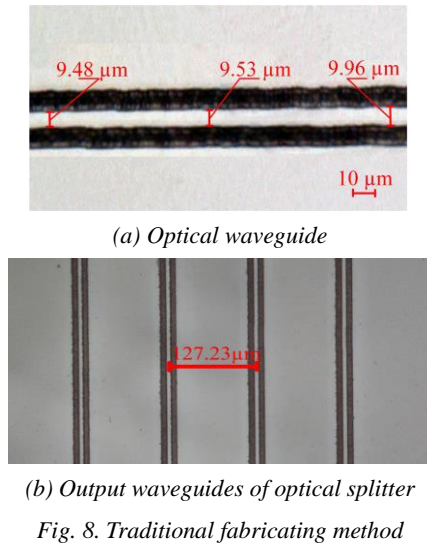
(a) Ablated linewidth



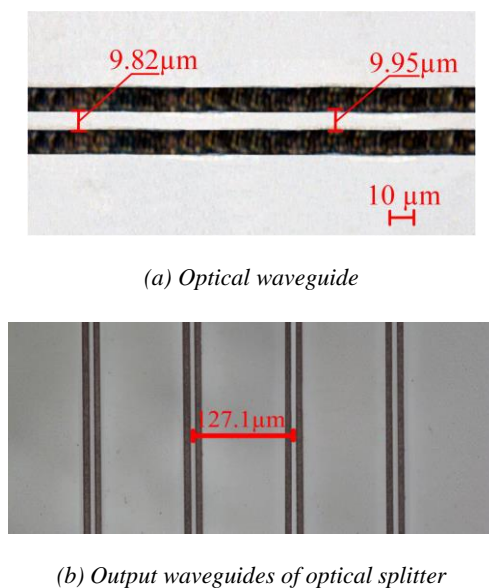
(b) Ablated depth

Fig. 7. The results of cross-experiments (color online)

When laser power and translational speed were ($90\ \text{mW}$, $15\ \text{mm/s}$) and ($110\ \text{mW}$, $20\ \text{mm/s}$), the ablated linewidth were $4.08\ \mu\text{m}$ and $4.12\ \mu\text{m}$, respectively. Similarly, when laser power and translational speed were ($70\ \text{mW}$, $15\ \text{mm/s}$) and ($90\ \text{mW}$, $15\ \text{mm/s}$), the ablated depth were $9.80\ \mu\text{m}$ and $10.08\ \mu\text{m}$ after scan once, respectively. In these results, laser power $90\ \text{mW}$ and translational speed $15\ \text{mm/s}$ were simultaneously selected.



An optical splitter was manufactured by traditional fabricating method with light path 2. Linewidths were obtained, which were 9.96 μm , 9.53 μm and 9.48 μm in Fig. 8(a), respectively. The extreme difference of linewidth was less than 0.5 μm , and edges of optical splitter were not very smooth. The spacing of output waveguides was about 127.23 μm in Fig. 8(b). Another optical splitter was manufactured with composite fabricating method. The simultaneous spatial and temporal focusing technology was used, laser power was 0.6 mW, ablated diameter was almost 0.29 μm and ablated depth was almost 10 μm on the Su8 adhesive by single pulse. When translational speed was 1.125 mm/s, linewidths were obtained, which were 9.95 μm , 9.82 μm in Fig. 9(a), respectively. The extreme difference of linewidth was less than 0.15 μm , the spacing of output waveguides was 127.1 μm , and their edges were smoother in Fig. 9(b).



The 45° coupled waveguide structure was manufactured with light path 1. The laser processing path was as shown in Fig. 10(b), laser focus diameter was approximately equal to 0.3 μm (focus diameter $S_d = 0.3 \mu\text{m}$). Laser focus was attached to the silica substrate and it was ablated once along Z direction at a speed of 1.125 mm/s. After this ablation, the laser focus was raised of 30 μm along Y direction, it returned to the starting plane along -Z direction, then, the laser focus was lowered of 30 μm along -Y direction, and laser focus returned to the starting position. Again, laser focus was moved 0.1 μm along -X and Y directions simultaneously, and was ablated once along Z direction at a speed of 1.125 mm/s. Similarly, laser focus returned to the starting position of second ablating. Next time, laser focus would move 0.1 μm (moving step size $S_x=S_y=0.1\mu\text{m}$) again along -X and Y directions, and ablated once at a speed of 1.125 mm/s. Similarly, laser focus would return to the starting position of third ablating. According to these ablating steps, the 45° waveguide coupled structure was fabricated. Then, ablation was run again according to the computer program. The final 45° waveguide coupled structure could be fabricated in Fig. 10(c). The thickness of 45° coupled waveguide structure was about 9.9 μm , and the angle was about 45.5°. Ra was approximately equal to 0.2 μm .

Traditional fabricating method was also theoretically similar, except that laser power, translational speed, the number of scan and moving step size were different. Laser focus diameter was approximately equal to 3.25 μm ($S_d = 3.25 \mu\text{m}$). Laser power was 10 mW, ablating depth was about 3.3 μm after scan once. Laser focus was also attached to the silica substrate and it was ablated three times along Z direction at a speed of 30 mm/s. After this ablation, the laser focus was also raised of 30 μm along Y direction, it returned to the starting plane along -Z direction, then, the laser focus was lowered of 30 μm along -Y direction, and laser focus returned to the starting position. Again, laser focus was moved 1 μm along -X and Y directions simultaneously, and was ablated three times along Z direction at a speed of 30 mm/s. Similarly, laser focus returned to the starting position of second ablating. Next time, laser focus would move 1 μm (moving step size $S_x=S_y=1\mu\text{m}$) again along -X and Y directions, and ablated three times at a speed of 30 mm/s. Similarly, laser focus would return to the starting position of third ablating. Then, ablation was still run again according to the computer program. The final 45° waveguide coupled structure could be fabricated in Fig. 10(a). The thickness of 45° coupled waveguide structure was about 9.91 μm , and the angle was about 45.8°. Ra was approximately equal to 0.5 μm . It could be clearly seen that the composite fabricating method was more effective than traditional fabricating method, and the ablated angle was more accurate and closer to 45°. In addition, the surface roughness of ablated angle was even smaller and could reach Ra 0.2 level.

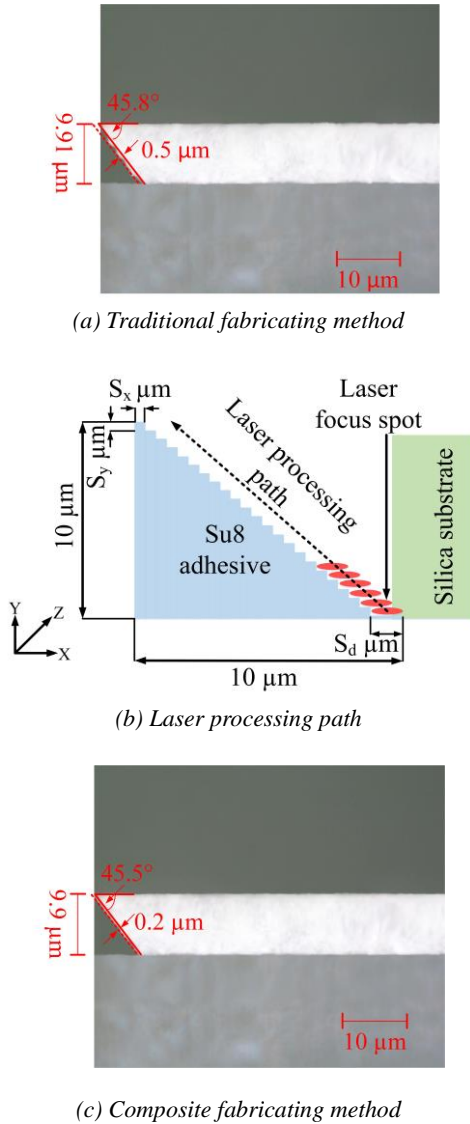


Fig. 10. 45° coupled waveguide structure and laser processing path (color online)

A 1×16 MMI vertical coupling optical splitter was fabricated by composite fabricating method. The length of optical splitter was 2.199 cm, the length difference was 0.001 cm, it would not affect the light transmission performance in Fig. 11(b). The spacing of output ports of MMI part was about 20.03 μm , the width of output waveguide was approximately equal to 9.95 μm , and the width of MMI part was 40.05 μm in Fig. 11(a). The width of input waveguide was about 9.97 μm , and the width of MMI part was approximately equal to 40.07 μm in Fig. 11(c). Three-dimensional morphology of MMI output port was shown in Fig. 11(d), it clearly reflected the details of part (I) in Fig. 11(a). It could be seen that the width of output optical waveguide was about 9.95 μm , the depth was about 9.93 μm , and the distance between two output waveguides was about 20 μm . And the surface and edges were almost smooth. The hypotenuse was steeper. Similarly, three-dimensional morphology of

MMI input port was shown in Fig. 11(e), it showed the details of part (II) in Fig. 11(c). It could be seen that the width of output optical waveguide was about 9.97 μm , the depth was about 9.95 μm , and the surface and edges were relatively smooth. The hypotenuse was also steeper.

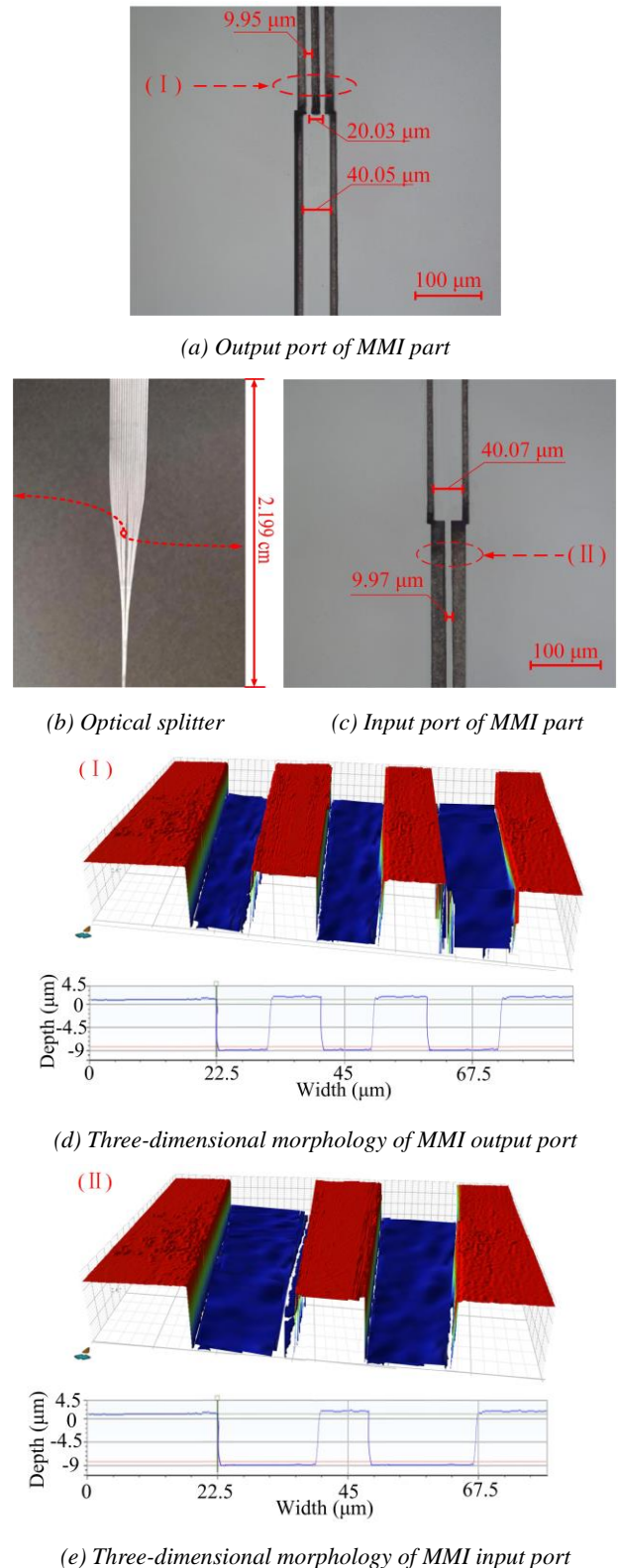


Fig. 11. Details of the optical splitter (color online)

The optical fiber coupling method was used to test the insertion loss [44-45] of optical splitter. The laser was coupled to the input port of optical splitter through the single mode fiber. The output end of optical splitter was coupled to the receiving end of optical power meter by the multimode fiber. The insertion loss could be obtained by the formula.

$$IL_i = -10 \log_{10} \frac{P_{out_i}}{P_{in}} \quad (i = 1, 2, 3, \dots, N) \quad (17)$$

Here, P_{out_i} was the optical power of output port, P_{in} was the optical power of input port.

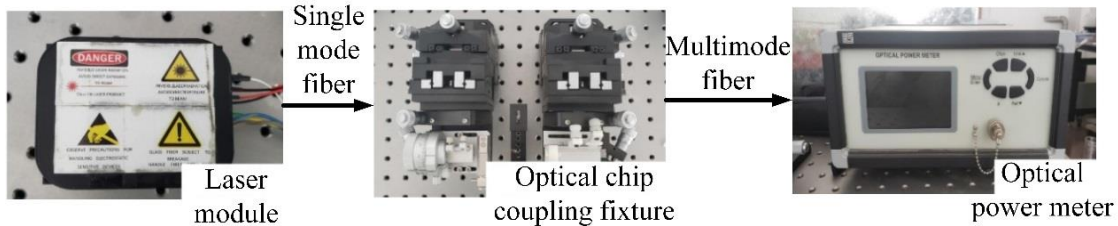


Fig. 12. Insertion loss test system

The performance of 1×16 MMI vertical coupling optical splitters were compared in Fig. 13, which were fabricated by traditional fabricating method and by composite fabricating method, respectively. After 15 sets of experiments, average insertion loss of output ports was 18.34 dB and non-uniformity was 0.1988 by composite fabricating method. However, average insertion loss of output ports was 21.32 dB and non-uniformity was 0.2314 by traditional fabricating method.

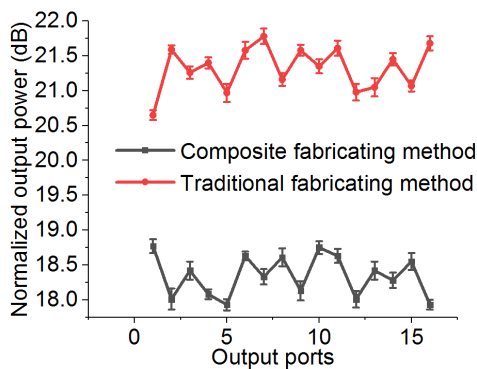


Fig. 13. Average insertion loss of each output port

It could be seen that average insertion loss of each output port reduced 2.98 dB and non-uniformity reduced 0.0326 with composite fabricating method in above results. The performance of optical splitter fabricated by composite fabricating method was better than that of optical splitter fabricated by traditional fabricating method.

Non-uniformity [46-47] was defined as the ratio of the minimum output optical power to the maximum optical power at these output ports. Its expression was,

$$ILu = -10 \log_{10} \frac{P_{out_{min}}}{P_{out_{max}}} \quad (18)$$

Here, $P_{out_{min}}$ was the minimum output optical power, $P_{out_{max}}$ was the maximum optical power. The smaller was the non-uniformity, the better was the device performance. The insertion loss test system was shown in Fig. 12.

5. Conclusions

In this paper, a 1×16 MMI vertical coupling optical splitter with Su8 core layer and air cladding was designed and fabricated by femtosecond laser composite fabricating method. The simulation results showed that the cladding of optical splitter was air with refractive index of 1@1550 nm. The substrate of SiO_2 with refractive index of 1.45@1550 nm. The core layer of Su8 adhesive with refractive index of 1.566@1550 nm. And, the cross-section of optical waveguide was $10 \mu\text{m} \times 10 \mu\text{m}$. The length of optical splitter was 2.2 cm, the spacing of output waveguide branches was $127 \mu\text{m}$, average insertion loss was 16.53 dB, and non-uniformity was 0.0486 dB. Only when $\theta \in [44.8^\circ \ 45.9^\circ]$, δ was greater than 90%.

Fabricating results showed that length of optical splitter was 2.199 cm, and the spacing of output waveguide branches was about $127.1 \mu\text{m}$. The thickness of 45° coupled waveguide structure was about $9.9 \mu\text{m}$, and the angle was about 45.5° . Ra was approximately equal to $0.2 \mu\text{m}$. The spacing of output ports of MMI part was about $20.03 \mu\text{m}$, the width of output waveguide was approximately equal to $9.95 \mu\text{m}$, the depth was about $9.93 \mu\text{m}$, and the average width of MMI part was about $40.06 \mu\text{m}$. The width of input waveguide was about $9.97 \mu\text{m}$, the depth was about $9.95 \mu\text{m}$. The average insertion loss of output ports was 18.34 dB, and the non-uniformity was 0.1988 dB. These values met requirements of vertical coupling optical interconnection for the EOPCB.

Acknowledgements

This work was supported by Hubei University of Technology Green Industry Technology Leading Project (CPYF2017002); Hubei University of Technology "Advanced Manufacturing Technology and Equipment" Collaborative Innovation Center Open Research Fund (1201501); Hubei University of Technology "Advanced Manufacturing Technology and Equipment" Collaborative Innovation Center Open Research Fund (1201803); Innovation and Entrepreneurship Training Program for College Students (S202010500100).

References

- [1] Qing Tao, Fengguang Luo, Lei Cao, Jian Guan, Jian Hu, Dusi Cai, Xiaokang Ye, *Optik* **122**, 1603 (2011).
- [2] Lars Brusberg, Simon Whalley, Christian Herbst, Henning Schröder, *Optics Express* **23**(25), 32528 (2015).
- [3] Takaaki Ishigure, Keishiro Shitanda, Yutaro Oizumi, *Optics Express* **23**(17), 22262 (2015).
- [4] K. K. Tung, W. H. Wong, E. Y. B. Pun, *Applied Physics A* **80**, 621 (2005).
- [5] E. Jordana, J.-M. Fedeli, P. Lyan, J. P. Colonna, P. Gautier, N. Daldosso, L. Pavesi, Y. Lebour, P. Pellegrino, B. Garrido, J. Blasco, F. Cuesta-Soto, P. Sanchis, 2007 4th IEEE International Conference on Group IV Photonics, (2007).
- [6] Yuqing Jiao, Tjibbe de Vries, Ralph-Stephan Unger, *Journal of the Electrochemical Society* **162**(8), E90 (2015).
- [7] G. Ulliac, V. Calero, A. Ndao, *Optical Materials* **53**, 1 (2016).
- [8] Sho Yakabe, Hitomi Matsui, Yui Kobayashi, *Journal of Lightwave Technology* **39**(2), 547 (2021).
- [9] Yui Kobayashi, Yoji Sakaguchi, Kazuki Yasuhara, Takaaki Ishigure, *Optics Express* **29**(6), 9513 (2021).
- [10] Yong Zhao, Hang Zhao, Ri-qing Lv, *Optics and Lasers in Engineering* **117**, 7 (2019).
- [11] Yuechen Jia, Shixiang Wang, Feng Chen, *Opto-Electronic Advances* **3**(10), 190042/1 (2020).
- [12] Lianchao ShangGuan, Daming Zhang, Tong Zhang, Ru Cheng, Jihou Wang, Chunxue Wang, Fei Wang, Seng-Tiong Ho, Changming Chen, Teng Fei, *Dyes and Pigments* **176**, 1 (2020).
- [13] Lilei Wang, Donghai Niu, Changming Chen, Zhiyong Li, Xibin Wang, *Optical Materials* **97** (article id.109386), 1 (2019).
- [14] Virginia Mansanares Giacon, Giovana da Silva Padilha, Julio Roberto Bartoli, *Optik* **126**, 74 (2015).
- [15] Krzysztof Nieweglowski, Lukas Lorenz, Sebastian Lungen, Tobias Tiedje, Klaus-Jürgen Wolter, Karlheinz Bock, *Microelectronics Reliability* **84**, 121 (2018).
- [16] F. Chen, J. R. Vázquez de Aldana, *Laser Photonics Rev.* **8**(2), 251 (2014).
- [17] Roberto Osellame, Giulio Ceruo, Roberta Ramponi, "Femtosecond Laser Micromachining: Photonic and Microfluidic Devices in Transparent Materials", Springer Science & Business Media, Heidelberg, Germany (2012).
- [18] Dezhi Tan, Zhuo Wang, Beibei Xu, Jianrong Qiu, *Adv. Photonics* **3**(2), 024002 (2021).
- [19] Felix Sima, Koji Sugioka, Rebeca Martínez Vázquez, Roberto Osellame, Lóránd Kelemen, Pal Ormos, *Nanophotonics* **7**(3), 613 (2018).
- [20] Zhuo-Chen Ma, Yong-Lai Zhang, Bing Han, Qi-Dai Chen, Hong-Bo Sun, *Small Methods* **2**(7), 1700413 (2018).
- [21] Bin Zhang, Lei Wang, Feng Chen, *Laser Photonics Rev.* **14**(8), 1900407 (2020).
- [22] Welm M. Pätzold, Ayhan Demircan, Uwe Morgner, *Opt. Express* **25**(1), 263 (2017).
- [23] M. De Vittorio, M. T. Todaro, T. Stomeo, R. Cingolani, D. Cojoc, E. Di Fabrizio, *Microelectronic Engineering* **73**, 388 (2004).
- [24] Fu-Hsiang Ko, Jem-Kun Chen, Feng-Chih Chang, *Microelectronic Engineering* **83**, 1132 (2006).
- [25] Vanga Sudheer Kumar, Shuvan Prashant Turaga, Ee Jin Teo, Andrew A. Bettiol, *Microelectronic Engineering* **102**, 33 (2013).
- [26] Lu Huang, Yaqiang Qin, Yunfeng Jin, Hao Shi, Honglian Guo, Liantuan Xiao, Yuqiang Jiang, *Nanophotonics* **9**(14), 4315 (2020).
- [27] Kaiming Zhou, Fangcheng Shen, Guolu Yin, Lin Zhang, *Optical Sensors SeW3D*, 1 (2016).
- [28] Daniel J. Heath, James A. Grant-Jacob, Matthias Feinaeugle, Ben Mills, Robert W. Eason, *Applied Optics* **56**(22), 6398 (2017).
- [29] Yuanhang Zhang, Mohammed A. Al-Mumin, Huiyuan Liu, Chi Xu, Lin Zhang, Patrick L. LiKamWa, Guifang Li, *Journal of Lightwave Technology* **37**(13), 01 (2019).
- [30] Yuxin Liang, Mingshan Zhao, Yuqing Luo, Yiying Gu, Yang Zhang, Linghua Wang, Xiyou Han, Zhenlin Wu, *Optical Engineering* **55**(11), 117102 (2016).
- [31] Andrea Zanzi, Antoine Brimont, Amadeu Griol, Pablo Sanchis, Javier Marti, *Optics Letters* **41**, 2 (2016).
- [32] Qing Tao, Fengguang Luo, Jing Yuan, Lu Shi, Jian Hu, Xu Ding, Ruifeng Wang, Lei Cao, *Optik* **122**, 76 (2011).
- [33] Qing Tao, Bowen Lu, Zhongsheng Zhai, Jian Cheng, Dun Liu, *Optical Engineering* **59**(01), 1 (2020).
- [34] Xiao Zhi-Gang, Li Bin-Cheng, *Opto-Electronic Engineering* **35**(8), 29 (2008).
- [35] Jung-Hwan Song, Jisu Kim, Hoon Jang, In Yong Kim, Indra Karnadi, Jonghwa Shin, Jung H. Shin, Yong-Hee Lee, *Nature Communications* **6**(7080), 1 (2015).
- [36] Carlos Doñate-Buendía, Mercedes

- Fernández-Alonso, Jesús Lancis, Gladys Mínguez-Vega, *Photonics Research* **7**(11), 1249 (2019).
- [37] Erica Block, Michael Greco, Dawn Vitek, *Biomedical Optics Express* **4**(6), 831 (2013).
- [38] J. Squier, J. Thomas, E. Block, C. Durfee, S. Backus, *Applied Physics A* **114**, 209 (2014).
- [39] Fei He, Ya Cheng, Jintian Lin, *New Journal of Physics* **13**(1), 083014 (2011).
- [40] Robert Kammel, Klaus Bergner, Jens U. Thomas, Roland Ackermann, Stefan Skupin, Stefan Nolte, *Laser-based Micro- & Nanoprocessing X, Proc. of SPIE* **9736**, 97360T-1 (2016).
- [41] L. Gallais, D.-B. Douti, M. Commandre, *Journal of Applied Physics* **117**, 223103 (2015).
- [42] Adrien Hervy, Laurent Gallais, Gilles Chériaux, *Optical Engineering* **56**(1), 011001 (2017).
- [43] Angelina Jaros, Jana Hartmann, Hao Zhou, *Scientific Reports* **8**, 11560 (2018).
- [44] Yipeng Song, Peipeng Xu, *Optics Communications* **426**, 30 (2018).
- [45] Keijiro Suzuki, Ryotaro Konoike, Junichi Hasegawa, Satoshi Suda, Hiroyuki Matsuura, Kazuhiro Ikeda, Shu Namiki, Hitoshi Kawashima, *Journal of Lightwave Technology* **37**(1), 116 (2019).
- [46] Stanislava Serecunova, Dana Seyringer, Frantisek Uherek, Heinz Seyringer, *Optics Communications* **501**, 127362 (2021).
- [47] Haojie Zhang, Noel Healy, Li Shen, *Scientific Reports* **6**(23512), 1 (2016).

*Corresponding author: 1910121219@hbut.edu.cn